International Journal of
Molecular Sciences

MDPI

Communication

Size Matters: Rethinking Hertz Model Interpretation for Cell Mechanics Using AFM

Katarína Mendová [1], Martin Otáhal [2], Mitja Drab [3] and Matej Daniel [1,*]

[1] Department of Mechanics, Biomechanics and Mechatronics, Faculty of Mechanical Engineering, Czech Technical University in Prague, Technická 4, 16000 Prague, Czech Republic; katarina.mendova@fs.cvut.cz
[2] Department of Natural Sciences, Faculty of Biomedical Engineering, Czech Technical University in Prague, Náměstí Sítná 3105, 27201 Kladno, Czech Republic; martin.otahal@fbmi.cvut.cz
[3] Laboratory of Biophysics, Faculty of Electrical Engineering, University of Ljubljana, Trzaska 25, 1000 Ljubljana, Slovenia; mitja.drab@fe.uni-lj.si
* Correspondence: matej.daniel@cvut.cz; Tel.: +420-224-352-518

Abstract: Cell mechanics are a biophysical indicator of cell state, such as cancer metastasis, leukocyte activation, and cell cycle progression. Atomic force microscopy (AFM) is a widely used technique to measure cell mechanics, where the Young modulus of a cell is usually derived from the Hertz contact model. However, the Hertz model assumes that the cell is an elastic, isotropic, and homogeneous material and that the indentation is small compared to the cell size. These assumptions neglect the effects of the cytoskeleton, cell size and shape, and cell environment on cell deformation. In this study, we investigated the influence of cell size on the estimated Young's modulus using liposomes as cell models. Liposomes were prepared with different sizes and filled with phosphate buffered saline (PBS) or hyaluronic acid (HA) to mimic the cytoplasm. AFM was used to obtain the force indentation curves and fit them to the Hertz model. We found that the larger the liposome, the lower the estimated Young's modulus for both PBS-filled and HA-filled liposomes. This suggests that the Young modulus obtained from the Hertz model is not only a property of the cell material but also depends on the cell dimensions. Therefore, when comparing or interpreting cell mechanics using the Hertz model, it is essential to account for cell size.

Keywords: atomic force microscopy (AFM); cell mechanics; cell stiffness; Hertz contact model

Citation: Mendová, K; Otáhal M.; Drab M.; Daniel M. Size Matters: Rethinking Hertz Model Interpretation for Cell Mechanics Using AFM. *Int. J. Mol. Sci.* **2024**, *25*, 7186. https://doi.org/10.3390/ijms25137186

Academic Editor: Demetrios A. Arvanitis

Received: 15 May 2024
Revised: 17 June 2024
Accepted: 25 June 2024
Published: 29 June 2024

1. Introduction

In the past 30 years, atomic force microscopy (AFM) has revolutionized the way we probe cell mechanics [1]. Originally developed to provide topographic images of solid surfaces [2], it is now routinely applied to measure the mechanical properties of individual cells [3]. AFM quantifies cell mechanics by applying a subtle but controlled force or displacement to a cell through a tiny tip and measuring the response with high precision [4].

Unlike other methods such as fluorescent microscopy, cryo-electron tomography, or three-dimensional electron microscopy, AFM allows cells to be studied without staining, labeling, or fixation, thus under physiological conditions [3]. Cell mechanics are observed to indicate cell biological functions such as adhesion, migration, or differentiation [1,5,6]. The mechanical properties of cells are also related to pathology, particularly metastatic cancer [7], cardiovascular disease [8], or infection by microbes or viruses [9].

During the development of the AFM technique, considerable effort was put into developing fast, accurate, and gentle microscopes. The high-speed imaging of living cells permits the study of drugs in surface cell structures [1] or the mechanical mapping of subcellular and subnuclear structures in real time [10]. Although progress in instrumentation and method has been considerable, little has changed in the processing and analysis of AFM results.

In mechanical analysis, the response of the material to external stimuli, such as applied fields or forces, is expressed by constitutive parameters [11]. These are quantities that are specific to each material. In theory, the constitutive parameters should be independent of the measurement instrument, sample, method, or model. In a first approximation, the cell could be considered a homogeneous isotropic elastic material and hence characterized by two parameters, e.g., Young's modulus E, and Poisson ratio ν [12]. Young's modulus describes how a cell material resists deformation when uniaxial stress is applied, while Poisson's ratio is a measure of how much the cell deforms in the lateral direction when compressed in the axial direction. Since the Poisson ratio of most soft biological tissues is very close to 0.5 [13] and the error in Young's modulus due to the unknown Poisson ratio is less than 10% [14], the cell mechanics are usually characterized only by the Young modulus [12].

The AFM provides a non-linear force/displacement curve even for elastic engineering materials that are conditioned by non-linear contact mechanics between the small tip and large sample. To extract the elastic modulus from AFM experiments, a model of contact mechanics is usually employed. The most common models are the Hertz and the Sneddon models for spherical and conical indenters, respectively [15,16]. The general description of indentation curve analysis was provided later by Pharr, Oliver, and Brotzen, 1992 [17].

It has been shown that both the Hertz model and Oliver–Pharr model provide identical results for purely elastic samples and for spherical indenters [18]. For the Hertz model, the dependence between the indentation force F and indentation depth h for a stiff spherical tip of radius R is expressed as [19]:

$$F = \frac{4}{3} E^* \sqrt{R} h^{3/2}$$

where E^* is the reduced Young modulus:

$$E^* = \frac{E}{1 - \nu^2}$$

The derivation of the Hertz model along with its assumptions are outlined in Appendix A. The basic assumptions of the Hertz model are that the strains are small and within the elastic limit, which means that the cell material behaves linearly and recovers its original shape after the contact; the surfaces of the cell and indenter are continuous and nonconforming, which means that the contact area is much smaller than the characteristic dimensions of the cell and the tip; the cell surface is frictionless, which means that there is no tangential force or shear stress between the surfaces of the AFM tip and cell; and the AFM tip is absolutely stiff with the shape of an exact sphere, which means that deformations of the tip and substrate are negligible compared to cells. Deviation from these assumptions in live cells given by the geometry, composition, and material heterogeneity of the cells brings additional variability into the estimated Young's modulus [20]. It is further assumed that if the cell is much larger than the depth of indentation, the stresses induced by loading vanish far from the indentation point. As shown in Appendix A, this assumption considers the cell to be an elastic half-space, meaning the cell volume is infinitely large compared to the area of contact. The elastic half-space assumption is a cornerstone for both the Hertz and Oliver–Pharr models [21].

Although theoretical and experimental studies based on elastic shell theory [22] and liquid drop theory [23] suggest that cell stiffness is considerably affected by its dimensions, this factor is neglected in Hertz theory. We hypothesize that larger cells will have lower stiffness and therefore a smaller Young's modulus, and vice versa. To minimize the effect of mechanical and shape variability between individual cells, we will use liposomes as cell models and evaluate Young's modulus by fitting the standard Hertz model to the experimental AFM force/deflection curves as outlined in Figure 1.

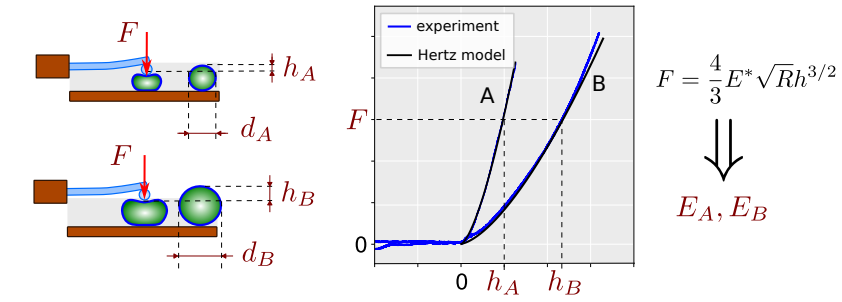

Figure 1. Overview of study: AFM measurement of liposomes of various sizes: A small diameter, B large diameter; curves fitting with Hertz contact model; estimation of Young's modulus of elasticity as fitting parameter.

2. Results

The Hertz model provides a good fit to the AFM data as evidenced by the high correlation coefficient between the measured and predicted values (Pearson correlation coefficient mean 0.998 for all measurements, range 0.9881–0.999). Representative loading curves are presented in Figure 2. Young's modulus in HA-filled liposomes (mean 1.11 kPa, range 0.30–1.85 kPa) is significantly higher than in PBS-filled liposomes (mean 0.37 kPa, range 0.62–1.28 kPa) (Wilcoxon rank sum test, $W = 423$, $p < 0.001$). The higher stiffness in HA-filled liposomes corresponds to steeper force/deflection curves (Figure 2). The results showed a high degree of agreement between repeated measurements as indicated by the low variation between the measured curves and in the estimated Young modulus (Figures 2 and 3).

Linear regression was used to test whether the liposome size significantly predicts Young's modulus. For both liposomes filled with PBS and HA, the effect of the liposome diameter d is statistically significant and negative ($\beta = -23.44$, 95% CI [−28.33, −18.56], $p < 0.001$ for the liposome filled with PBS and $\beta = -36.53$, 95% CI [−45.58, −27.48], $p < 0.001$ for liposomes filled with HA). The effect of the diameter of the liposome on Young's modulus is significantly higher for HA-filled liposomes (ANOVA $p = 0.008$).

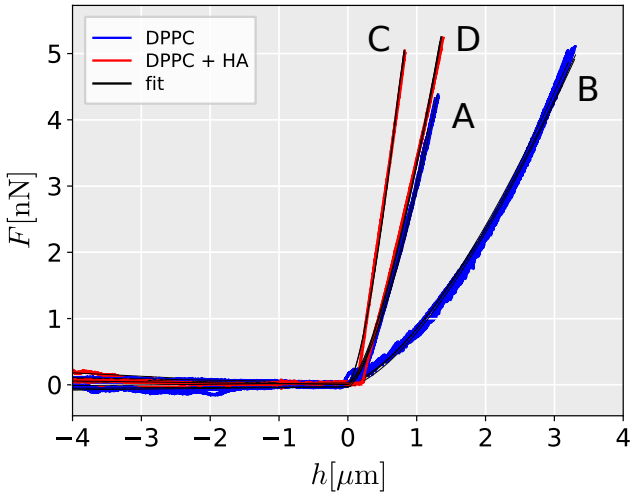

Figure 2. Measured indentation curve for DPPC liposomes in PBS filled with (DPPC) PBS and (DPPC + HA) HA solution. The fit of indentation by the Hertz contact model for the hemispherical AFM tip is shown. Refer to Figure 3 for details on individual liposomes properties (capital letters).

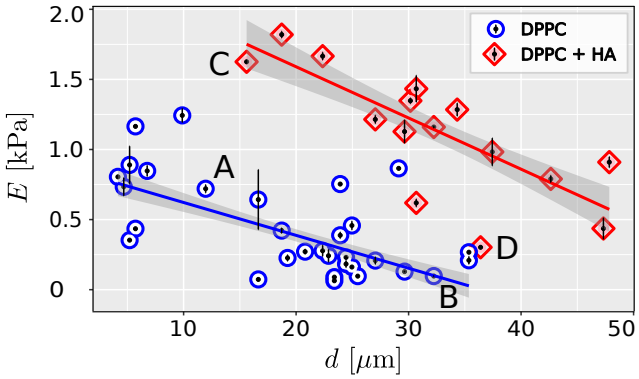

Figure 3. Linear regression plot with 95% confidence intervals (shaded areas) showing measured dependence between the size of DPPC liposomes and Young's modulus estimated from Hertz model. Measured data along with the range of measured values are shown for liposomes filled with PBS and HA solution, denoted as DPPC and DPPC + HA, respectively. Indentation curves for selected liposomes A-D are shown in Figure 2.

3. Discussion

One of the primary assumptions of the Hertz model for analyzing contact mechanics is that the cell is elastic, isotropic, and homogeneous, and that the indentation is small compared to the size of the cell [19]. In this study, we evaluated the effect of cell size on the estimated Young's modulus using liposomes as cell models, and adopting methods proposed for cell mechanics measurements [24]. We demonstrated a significant dependence between the size of the measured liposome and its stiffness (Figures 2 and 3).

Our findings are consistent with previous studies by Delorme et al. (2006) [25], who observed higher stiffness in smaller liposomes. The observed size effect of liposomes aligns with the shell theory of cell deformation [26,27]. Real-time deformability cytometry also indicates greater deformation for larger cells of the same phenotype [28] as observed in our study.

The scattering of data in Figure 3 suggests the influence of additional factors on the measured mechanical response. One such factor that warrants further evaluation is liposome adhesion. Theoretical [29] and experimental studies [30] have shown that extensive cell adhesion increases cell membrane tension and stiffness. AFM measurements also indicate that the stiffness of adherent epithelial cells increases with the projected area of apical cells [31]. Hence, liposomes with significant adhesion to the surface were excluded from our analysis. Overbeck et al. (2017) demonstrated that osmotic pressure can also affect cell response, with higher osmolarity contributing to decreased cell stiffness [23].

For spherical probes, it has been reported that the sample can be considered an elastic half-space if the indenter's radius is at least ten times smaller than each horizontal dimension of the sample [15]. The Oliver–Pharr indentation analysis further suggests that the Hertz model is applicable for spherical indenters when the h/R ratio is less than 10 [18]. Modifications to the Hertz model have been proposed to introduce correction factors for substantial deformations [18].

The presented results were obtained using liposomes as cell models, which reduces variability in input parameters by employing experimental samples with controlled composition and geometry. While liposomes mimic basic cell structures, they may not fully capture the active behavior of living cells. Cells are heterogeneous structures with intricate internal organization. For instance, the anisotropy of the cytoskeleton induces non-axisymmetric deformations [32], and the stiffness of subcellular structures influences local mechanical responses [10]. The prolonged or repeated indentation of single cells can lead to cytoskeletal remodeling [33], which further impacts cell stiffness. When measuring live cells, active responses due to cytoskeletal remodeling should also be considered [34]. The experimental model could be enhanced by incorporating self-assembled actin shells [35].

To create a more realistic artificial cell model, we tested HA-filled liposomes. The high molecular weight and semi-flexible chain of HA impart viscous and elastic properties [36], akin to those observed in the cytoplasm [37]. The viscosity of the HA solution used (100 Pa s) [38] corresponds to the viscosity of cell cytoplasm [39]. The addition of HA, mimicking cytoplasm, increases the effect of cell size on the estimated Young's modulus. Our results underscore the importance of considering the internal environment in modeling cell mechanics. Further research is needed to quantify the relationship between cell size and stiffness in confluent and highly adherent living cells with complex internal organization.

4. Materials and Methods

4.1. Liposomes Preparation

Liposomes are prepared using a two-stage microfluidic device that produces filled liposomes using the double emulsion drop method. The custom-made microfluidic device is manufactured using PolyJet technology (Polyjet J750, Stratasys, Eden Prairie, MN, USA) from VeroClear-RGD810. The device consists of an inner aqueous phase channel, two lipid-carrying organic phase channels, an intermediate channel, two outer aqueous phase channels, and a downstream channel [40]. Using volume-controlled flow pumps, the inner aqueous stream of HA (molecular weight 2000–2200 kDa, concentration 5:1, Contipro, DolníDobrouč, Czechia) is dissolved in PBS (200 mL) for filled liposomes or PBS (10 mL) for PBS-filled liposomes. The surrounding lipid-carrying streams (DPPC in isopropyl alcohol, Sigma-Aldrich, Burlington, MA, US) are hydrodynamically focused, and a single emulsion droplet is formed by shearing the inner phase. Subsequently, a double emulsion is formed by two external streams of aqueous PBS (10 mL). As the aim of the study is to produce liposomes of various sizes, the diameter of the inner channel is 0.5 mm, allowing the formation of multidispersed liposomes. Liposome formation is driven by shear flow at the junctions by setting the individual flow rate ratio at 5, 10 and 15 mL/h for phospholipids, inner fluid and outer fluid, respectively. Liposome formation and flow focusing are inspected in situ using a phase microscope (NIB-100 Inverted Microscope with Canon SCR Camera, Canon, Tokyo, Japan).

4.2. Liposomes Fixation

The binding required to measure the mechanical properties of liposomes by AFM was achieved using an avidin–biotin complex. Biotin–DOPE and DPPC lipids were used at a concentration ratio of 1:1000. The biotinylated surface was incubated with avidin (0.30 mg/mL) and washed three times with PBS buffer. Subsequently, 1 mL of the liposomal formulation and approximately 1 mL of PBS buffer were applied to a Petri dish and incubated for 5 min at room temperature [41,42].

4.3. AFM Measurements

Mechanical testing of the liposomes was performed using the NanoWizard® 3 NanoOptics AFM System (JPK, DE). A colloidal probe with a diameter of 5.2 µm and a spring constant of 0.0307 N/m (APPnano, Mountain View, CA, USA) was employed. The cantilever was calibrated according to the manufacturer's standard procedure. First, the sensitivity of the cantilever was determined via indentation measurements on glass, followed by determining the stiffness using thermal noise analysis. Force spectroscopy of the liposomes was performed with a z length of 15 µm, a relative set point of 20 nN, and a loading rate of 3.75 µm/s.

The following inclusion criteria were applied: the isolated spherical shape of the liposome without collapse [43] or extensive adhesion to the surface [44], and at least two successful measurements per liposome. Force/deformation curves were measured at the center of each liposome.

4.4. Data Processing

After subtracting the deflection of the cantilever, the force/displacement curves were fitted using the Hertz model for a hemispherical cantilever tip with and cell Poisson ratio of 0.5, according to the method described by Thomas et al. (2013) [24]. Data indicating strong attachment of liposomes to the surface (small height compared to diameter), liposome burst (rapid change in force), or extensive noise (AFM tip fouling) were excluded from the analysis. The final analysis included 162 measurements (116 and 46 in PBS- and HA-filled liposomes, respectively) across 46 liposomes (31 and 15 in PBS- and HA-filled liposomes, respectively).

4.5. Statistical Analyses

Statistical analyses were performed using R software (version 4.1.2, R Core Team, 2021). A p value less than 0.05 was considered statistically significant. The normality of the data was tested using the Shapiro–Wilk test. Differences in Young's modulus between different liposome types or treatments were analyzed using one-way analysis of variance (ANOVA), followed by Tukey's post hoc test for normally distributed data, and by the Wilcoxon rank sum test otherwise. The correlation between Young's modulus and cell size was assessed using linear regression (package lme4), considering repeated measurements [45]. In total, 95% confidence intervals (CI) and p values were calculated using a Wald t distribution approximation.

5. Conclusions

Atomic force microscopy (AFM) provides estimations of cellular stiffness. To attain statistical robustness in the analysis of highly heterogeneous cellular populations, a comprehensive examination of numerous individual cells is essential [46]. Moreover, the versatility of AFM encompasses the determination of cellular states through assessments at the single-cell level [47]. Enhancing the reliability of single-cell mechanics techniques necessitates the identification of potential variability sources among cells. Variability arises not only from physiological disparities but also from the methodologies employed in testing and subsequent data processing. Our empirical data suggest that cellular size, an aspect not accounted for in the foundational assumptions of the Hertz model, considerably influences the measured stiffness and the inferred Young's modulus. Consequently, for comparative analyses, it is advisable to select cells with commensurate dimensions. Further research is required to develop a correction factor tailored to the unique characteristics of living cells with complex internal structures.

Author Contributions: Conceptualization, M.D. (Matej Daniel) and K.M.; methodology, M.O.; software, M.D. (Mitja Drab); validation, K.M. and M.D. (Mitja Drab); formal analysis, M.D. (Matej Daniel); investigation, K.M. and M.D. (Mitja Drab); resources, M.D. (Matej Daniel); data curation, M.D. (Matej Daniel); writing—original draft preparation, M.D. (Matej Daniel); writing—review and editing, K.M. and M.O.; visualization, K.M.; funding acquisition, M.D.(Matej Daniel). All authors have read and agreed to the published version of the manuscript.

Funding: This research was funded by the Grant Agency of the Czech Technical University in Prague, grant No. SGS22/149/OHK2/3T/12.

Data Availability Statement: The original data presented in the study are openly available in Zenodo at https://zenodo.org/doi/10.5281/zenodo.11198627.

Conflicts of Interest: The authors declare no conflicts of interest.

Appendix A. On Derivation of Hertz Contact Theory for AFM Measurements Evaluation

The Hertz contact equations used to evaluate cell mechanics—relating the size of the contact area, the loading force, and the elastic compression—are rarely derived in studies related to AFM measurements. An accurate description of the Hertz equations falls within the field of contact mechanics. The theoretical description of the contact problem [19] makes the derivation challenging for a general audience, except for mathematicians and theoretical mechanicians. Although the final equations are relatively simple, their derivation is not straightforward.

For the sake of simplicity, we will further consider the simplest yet relevant problem to cell mechanics: a spherical indenter in contact with an elastic cell. The Hertzian contact pressure can be derived from the theory of elasticity based on the following assumptions [48,49]:

- The size of the cell is much larger than the size of the indenter, allowing the cell surface to be considered flat relative to the indenter.
- The spherical indenter is considered a rigid body, meaning it maintains its shape under loading.
- The cell in contact is considered homogeneous, meaning it possesses uniform qualities at different sites or consistent properties with increasing depth.
- The cell is isotropic, meaning it has identical properties in all directions.
- The displacements and stresses must satisfy the differential equations of equilibrium for elastic bodies, and the stresses must vanish at a great distance from the contact surface.
- The indenter and the cell are in frictionless contact.
- The surfaces of both the cell and the indenter have negligible roughness.
- At the surface of the bodies, the normal pressure is zero outside the contact area and equal and opposite inside the circle of contact.
- The distance between the surfaces of the two bodies is zero inside the circle of contact and greater than zero outside it.
- The weight of both the indenter and the cell is neglected.

In the following, we will present two methods for deriving the Hertz equations, highlighting the assumptions described above. The first method will offer a conceptual derivation as proposed by Johnson (1982) [50], while the second method will follow a more rigorous approach based on Boussinesq's problem as typically described in contact mechanics textbooks [19,48,51,52].

Appendix A.1. Hertz Contact Theory—Conceptual Solution

As the contact problem is axisymmetrical along the z axis, it is suitable to define the r coordinate as the radial distance from the axis of symmetry (Figure A1). The size of the contact zone in radial coordinates is denoted as a. At the surface of the cell, the normal pressure is zero outside the contact zone. Maximum deformation occurs under the loading force at $r = 0$. The relationship between the contact zone size a and the maximum deformation within the contact zone is defined geometrically as:

$$(R - h)^2 + a^2 = R^2 \tag{A1}$$

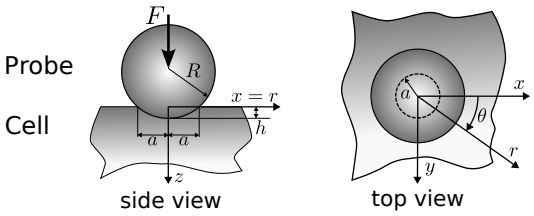

Figure A1. Geometry of contact between spherical indenter and cell.

If we assume that the deformation is much smaller than the size of the contact zone ($d \ll a$), we may express

$$h = \frac{a^2}{2R} \tag{A2}$$

The deformation can be defined as a dimensionless quantity:

$$\frac{h}{a} = \frac{a}{2R} \tag{A3}$$

An overview of the derivation of the Hertz equations was proposed by Johnson, 1982. If the cell behaves as an elastic body, the cell deformation depends on the stress and the material stiffness:

$$\frac{a}{R} \propto \frac{\overline{p}}{E^*} \tag{A4}$$

where $\overline{p}$ is the average contact pressure, and E^* corresponds to the material stiffness. For the spherical indenter and the definition of mean pressure, it holds that:

$$F = \pi a^2 \overline{p} \tag{A5}$$

Thus, combining Equations (A4) and (A5), we obtain:

$$F \propto \pi E^* \frac{a^3}{R} \tag{A6}$$

From the geometry of contact given by Equation (A1), it follows that:

$$F \propto \pi E^* \sqrt{R} h^{3/2} \tag{A7}$$

The elasticity constant E^* should reflect the plane strain as discussed below in the rotationally symmetric problem. For the plane strain, the equivalent elasticity modulus can be expressed as:

$$E^* = \frac{E}{1 - \nu^2} \tag{A8}$$

where ν is Poisson's ratio. Although the analysis in Equations (A1)–(A7) is formally correct, it does not provide the proportionality constants. To obtain the exact expression, one must adopt the principles of elasticity analysis. Further, it neglects the deformation outside the contact zone.

Appendix A.2. Boussinesq's Problem

To rigorously derive the treatment of contact, we adopt a simplified approach inspired by Hertz's method in his seminal paper [53]. This approach is based on what is known as Boussinesq's problem, which addresses the stresses and deformations within an elastic half-space caused by isolated force [54] (Figure A2). An elastic half-space is an idealized infinite object constrained by a single infinite plane.

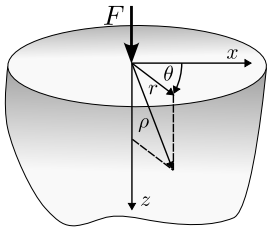

Figure A2. Boussinesq's problem.

The coordinate system is defined such that the x, y plane coincides with the free surface of the medium, and the z-axis points towards the elastic object. The origin of the coordinate system coincides with the point of action of the isolated force.

The geometry of the problem is axisymmetric, and thus the force induces axisymmetric loading. For such loading, the state can be described by the plane strain condition of deformation [55]:

$$\boldsymbol{u} = (u_r, 0, u_z) \tag{A9}$$

where u_r and u_z are displacements in the axisymmetric polar coordinates. The strain tensor is given by:

$$\boldsymbol{\epsilon} = \begin{pmatrix} \frac{\partial u_r}{\partial r} & 0 & \frac{1}{2}\left(\frac{\partial u_r}{\partial z} + \frac{\partial u_z}{\partial r}\right) \\ 0 & \frac{u_r}{r} & 0 \\ \frac{1}{2}\left(\frac{\partial u_r}{\partial z} + \frac{\partial u_z}{\partial r}\right) & 0 & \frac{\partial u_z}{\partial z} \end{pmatrix} \tag{A10}$$

The stress tensor is defined as:

$$\boldsymbol{\sigma} = \begin{pmatrix} \sigma_{rr} & 0 & \sigma_{rz} \\ 0 & \sigma_{\theta\theta} & 0 \\ \sigma_{rz} & 0 & \sigma_{zz} \end{pmatrix} \tag{A11}$$

Assuming linear elastic behavior of the material, the stress–strain relation is given by Hooke's law:

$$\boldsymbol{\sigma} = \lambda \mathrm{tr}(\boldsymbol{\epsilon})\boldsymbol{I} + 2\mu\boldsymbol{\epsilon} \tag{A12}$$

where λ and μ are Lame's constants, and $\boldsymbol{I}$ is the identity tensor. Neglecting body forces, the equations of equilibrium can be expressed as [19]:

$$\nabla \cdot \boldsymbol{\sigma} = \boldsymbol{0} \tag{A13}$$

where ∇ is the divergence operator. These differential equations can be solved using various methods, such as limiting cases of general normal loading, Kelvin's solution for a point force within an infinite space, or integral transform techniques (e.g., Love's strain function) [56].

In the analysis of cell deformation, the z-displacement is typically the only component considered. From the mathematical analysis of Boussinesq's problem, the displacement is obtained as [57]:

$$u_z = \frac{1+\nu}{2\pi E}\left[\frac{2(1-\nu)}{\rho} + \frac{z^2}{\rho^3}\right]F \tag{A14}$$

where $\rho = \sqrt{x^2 + y^2 + z^2}$. For surface deformation ($z = 0$), this simplifies to:

$$u_z = \frac{1-\nu^2}{\pi E}\frac{1}{r}F \tag{A15}$$

If the force F acts over a surface element, it can be expressed in axisymmetric coordinates:

$$p(r,\theta) = \frac{F(r,\theta)}{r\,\mathrm{d}\theta\,\mathrm{d}r} \tag{A16}$$

and the equation transforms to:

$$\mathrm{d}u_z = \frac{1-\nu^2}{\pi E}\frac{1}{r}p(r,\theta)r\,\mathrm{d}\theta\,\mathrm{d}r \tag{A17}$$

The contact problem can be decomposed into the superposition of deformations caused by individual forces acting simultaneously:

$$u_z(x,y) = \iint \frac{1-\nu^2}{\pi E}\frac{p(x',y')}{r'}\,\mathrm{d}x'\,\mathrm{d}y' \tag{A18}$$

where $r' = \sqrt{(x-x')^2 + (y-y')^2}$.

Appendix A.3. Hertz Contact Theory

The integral in Equation (A18) cannot be solved without knowing the stress distribution function. The pressure distribution can be represented as a shape function $p = p_0 f(r)$, where p_0 is the maximum contact pressure. Hertz (1882) [53] proposed that the pressure distribution in the contact area is given by

$$f(r) = \begin{cases} 0 & r \le a \\ \sqrt{1-(r/a)^2} & 0 < r < a \\ 1 & r = 0 \end{cases} \tag{A19}$$

The maximum deformation ($u_z(0,0) = h$, Figure A3) can be calculated from Equations (A17) and (A18) as:

$$h = \frac{2p_0}{E^*} \int_0^a \sqrt{1-\left(\frac{r}{a}\right)^2}\, \mathrm{d}r = \frac{\pi p_0 a}{2E^*} \tag{A20}$$

For other points, spherical symmetry dictates that deformations can be determined for any arbitrary point at distance r from the center, e.g., points lying on the x-axis. The position of an arbitrary point A on the x-axis is given in spherical coordinates as $[r, 0]$. The contribution of stress to deformation at such points depends on the radial distance from this point. A detailed derivation can be found in Popov, 2017 [52], where it is shown that:

$$u_z(r) = \frac{\pi p_0}{4aE^*}\left(2a^2 - r^2\right) \tag{A21}$$

Using Equation (A1) and setting $r = a$ in Equation (A21), we obtain for the size of contact area:

$$\frac{\pi p_0}{4E^*} a = h - \frac{a^2}{2R} \tag{A22}$$

$$a = \frac{\pi p_0 R}{2E^*} \tag{A23}$$

The contact radius is related to the deformation as:

$$a^2 = Rh \tag{A24}$$

The sum of all pressures over the contact area gives the resultant loading force:

$$F = \int_0^a \int_0^{2\pi} p_0 f(r) r \,\mathrm{d}\theta \,\mathrm{d}r = 2\pi p_0 \int_0^a \sqrt{1-\left(\frac{r}{a}\right)^2}\, r \,\mathrm{d}r = \frac{2}{3} p_0 \pi a^2 \tag{A25}$$

Substituting from Equations (A18)–(A25), we obtain:

$$F = \frac{4}{3} E^* \sqrt{R} h^{3/2} \tag{A26}$$

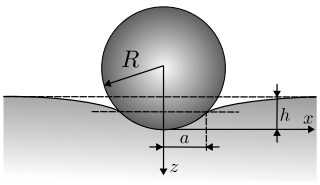

Figure A3. Schematic view of a rigid probe in contact with an elastic half-space.

References

1. Dufrêne, Y.F.; Viljoen, A.; Mignolet, J.; Mathelié-Guinlet, M. AFM in Cellular and Molecular Microbiology. *Cell. Microbiol.* **2021**, *23*, e13324. [CrossRef]
2. Binnig, G.; Quate, C.F.; Gerber, C. Atomic Force Microscope. *Phys. Rev. Lett.* **1986**, *56*, 930–933. [CrossRef]
3. Alsteens, D.; Beaussart, A.; El-Kirat-Chatel, S.; Sullan, R.M.A.; Dufrêne, Y.F. Atomic Force Microscopy: A New Look at Pathogens. *PLoS Pathog.* **2013**, *9*, e1003516. [CrossRef]
4. Moeendarbary, E.; Harris, A.R. Cell Mechanics: Principles, Practices, and Prospects. *Wiley Interdiscip. Rev. Syst. Biol. Med.* **2014**, *6*, 371–388. [CrossRef]
5. Wu, P.H.; Aroush, D.R.B.; Asnacios, A.; Chen, W.C.; Dokukin, M.E.; Doss, B.L.; Durand-Smet, P.; Ekpenyong, A.; Guck, J.; Guz, N.V.; et al. A Comparison of Methods to Assess Cell Mechanical Properties. *Nat. Methods* **2018**, *15*, 491–498. [CrossRef]
6. Li, M.; Dang, D.; Liu, L.; Xi, N.; Wang, Y. Atomic Force Microscopy in Characterizing Cell Mechanics for Biomedical Applications: A Review. *IEEE Trans. Nanobiosci.* **2017**, *16*, 523–540. [CrossRef] [PubMed]
7. Li, M.; Xi, N.; Wang, Y.C.; Liu, L.Q. Atomic Force Microscopy for Revealing Micro/Nanoscale Mechanics in Tumor Metastasis: From Single Cells to Microenvironmental Cues. *Acta Pharmacol. Sin.* **2021**, *42*, 323–339. [CrossRef]
8. Peña, B.; Adbel-Hafiz, M.; Cavasin, M.; Mestroni, L.; Sbaizero, O. Atomic Force Microscopy (AFM) Applications in Arrhythmogenic Cardiomyopathy. *Int. J. Mol. Sci.* **2022**, *23*, 3700. [CrossRef]
9. Ohnesorge, F.M.; Hörber, J.K.; Häberle, W.; Czerny, C.P.; Smith, D.P.; Binnig, G. AFM Review Study on Pox Viruses and Living Cells. *Biophys. J.* **1997**, *73*, 2183–2194. [CrossRef] [PubMed]
10. Efremov, Y.M.; Suter, D.M.; Timashev, P.S.; Raman, A. 3D Nanomechanical Mapping of Subcellular and Sub-Nuclear Structures of Living Cells by Multi-Harmonic AFM with Long-Tip Microcantilevers. *Sci. Rep.* **2022**, *12*, 529. [CrossRef] [PubMed]
11. Lim, C.T.; Zhou, E.H.; Quek, S.T. Mechanical Models for Living Cells—A Review. *J. Biomech.* **2006**, *39*, 195–216. [CrossRef]
12. Guz, N.; Dokukin, M.; Kalaparthi, V.; Sokolov, I. If Cell Mechanics Can Be Described by Elastic Modulus: Study of Different Models and Probes Used in Indentation Experiments. *Biophys. J.* **2014**, *107*, 564–575. [CrossRef]
13. Liu, B.; Zhang, L.; Gao, H. Poisson Ratio Can Play a Crucial Role in Mechanical Properties of Biocomposites. *Mech. Mater.* **2006**, *38*, 1128–1142. [CrossRef]
14. Dokukin, M.E.; Sokolov, I. On the Measurements of Rigidity Modulus of Soft Materials in Nanoindentation Experiments at Small Depth. *Macromolecules* **2012**, *45*, 4277–4288. [CrossRef]
15. Kontomaris, S.V.; Malamou, A.; Stylianou, A. The Hertzian Theory in AFM Nanoindentation Experiments Regarding Biological Samples: Overcoming Limitations in Data Processing. *Micron* **2022**, *155*, 103228. [CrossRef] [PubMed]
16. Sen, S.; Subramanian, S.; Discher, D.E. Indentation and Adhesive Probing of a Cell Membrane with AFM: Theoretical Model and Experiments. *Biophys. J.* **2005**, *89*, 3203–3213. [CrossRef] [PubMed]
17. Pharr, G.M.; Oliver, W.C.; Brotzen, F.R. On the Generality of the Relationship among Contact Stiffness, Contact Area, and Elastic Modulus during Indentation. *J. Mater. Res.* **1992**, *7*, 613–617. [CrossRef]
18. Kontomaris, S.V.; Malamou, A. Hertz Model or Oliver & Pharr Analysis? Tutorial Regarding AFM Nanoindentation Experiments on Biological Samples. *Mater. Res. Express* **2020**, *7*, 033001. [CrossRef]
19. Timoshenko, S.; Goodier, J.N. *Theory of Elasticity*; McGraw-Hill: New York, NY, USA, 1951.
20. Lekka, M.; Laidler, P. Applicability of AFM in Cancer Detection. *Nat. Nanotechnol.* **2009**, *4*, 72 [CrossRef] [PubMed]
21. Kontomaris, S.V.; Stylianou, A.; Malamou, A.; Stylianopoulos, T. A Discussion Regarding the Approximation of Cylindrical and Spherical Shaped Samples as Half Spaces in AFM Nanoindentation Experiments. *Mater. Res. Express* **2018**, *5*, 085402. [CrossRef]
22. Tsugawa, S.; Yamasaki, Y.; Horiguchi, S.; Zhang, T.; Muto, T.; Nakaso, Y.; Ito, K.; Takebayashi, R.; Okano, K.; Akita, E.; et al. Elastic Shell Theory for Plant Cell Wall Stiffness Reveals Contributions of Cell Wall Elasticity and Turgor Pressure in AFM Measurement. *Sci. Rep.* **2022**, *12*, 13044. [CrossRef] [PubMed]
23. Overbeck, A.; Günther, S.; Kampen, I.; Kwade, A. Compression Testing and Modeling of Spherical Cells – Comparison of Yeast and Algae. *Chem. Eng. Technol.* **2017**, *40*, 1158–1164. [CrossRef]
24. Thomas, G.; Burnham, N.A.; Camesano, T.A.; Wen, Q. Measuring the Mechanical Properties of Living Cells Using Atomic Force Microscopy. *J. Vis. Exp. JOVE* **2013**, *76*, 50497. [CrossRef]
25. Delorme, N.; Fery, A. Direct Method to Study Membrane Rigidity of Small Vesicles Based on Atomic Force Microscope Force Spectroscopy. *Phys. Rev. E* **2006**, *74*, 030901. [CrossRef]
26. Delorme, N.; Dubois, M.; Garnier, S.; Laschewsky, A.; Weinkamer, R.; Zemb, T.; Fery, A. Surface Immobilization and Mechanical Properties of Catanionic Hollow Faceted Polyhedrons. *J. Phys. Chem. B* **2006**, *110*, 1752–1758. [CrossRef]
27. Reissner, E. Stress Strain Relations in the Theory of Thin Elastic Shells. *J. Math. Phys.* **1952**, *31*, 109–119. [CrossRef]
28. Otto, O.; Rosendahl, P.; Mietke, A.; Golfier, S.; Herold, C.; Klaue, D.; Girardo, S.; Pagliara, S.; Ekpenyong, A.; Jacobi, A.; et al. Real-Time Deformability Cytometry: On-the-fly Cell Mechanical Phenotyping. *Nat. Methods* **2015**, *12*, 199–202. [CrossRef] [PubMed]
29. Ren, K.; Gao, J.; Han, D. AFM Force Relaxation Curve Reveals That the Decrease of Membrane Tension Is the Essential Reason for the Softening of Cancer Cells. *Front. Cell Dev. Biol.* **2021**, *9*, 663021. [CrossRef]
30. Xie, K.; Yang, Y.; Jiang, H. Controlling Cellular Volume via Mechanical and Physical Properties of Substrate. *Biophys. J.* **2018**, *114*, 675–687. [CrossRef]

31. Nehls, S.; Nöding, H.; Karsch, S.; Ries, F.; Janshoff, A. Stiffness of MDCK II Cells Depends on Confluency and Cell Size. *Biophys. J.* **2019**, *116*, 2204–2211. [CrossRef]
32. Efremov, Y.M.; Velay-Lizancos, M.; Weaver, C.J.; Athamneh, A.I.; Zavattieri, P.D.; Suter, D.M.; Raman, A. Anisotropy vs Isotropy in Living Cell Indentation with AFM. *Sci. Rep.* **2019**, *9*, 5757. [CrossRef] [PubMed]
33. Reed, J.; Troke, J.J.; Schmit, J.; Han, S.; Teitell, M.A.; Gimzewski, J.K. Live Cell Interferometry Reveals Cellular Dynamism During Force Propagation. *ACS Nano* **2008**, *2*, 841–846. [CrossRef] [PubMed]
34. Rajagopal, V.; Holmes, W.R.; Lee, P.V.S. Computational Modeling of Single-Cell Mechanics and Cytoskeletal Mechanobiology. *Wires Syst. Biol. Med.* **2018**, *10*, e1407. [CrossRef] [PubMed]
35. Lopes dos Santos, R.; Campillo, C. Studying Actin-Induced Cell Shape Changes Using Giant Unilamellar Vesicles and Reconstituted Actin Networks. *Biochem. Soc. Trans.* **2022**, *50*, 1527–1539. [CrossRef] [PubMed]
36. Cowman, M.K.; Schmidt, T.A.; Raghavan, P.; Stecco, A. Viscoelastic Properties of Hyaluronan in Physiological Conditions. *F1000Research* **2015**, *4*, 622. [CrossRef] [PubMed]
37. Xie, J.; Najafi, J.; Le Borgne, R.; Verbavatz, J.M.; Durieu, C.; Sallé, J.; Minc, N. Contribution of Cytoplasm Viscoelastic Properties to Mitotic Spindle Positioning. *Proc. Natl. Acad. Sci. USA* **2022**, *119*, e2115593119. [CrossRef]
38. Rebenda, D.; Vrbka, M.; Čípek, P.; Toropitsyn, E.; Nečas, D.; Pravda, M.; Hartl, M. On the Dependence of Rheology of Hyaluronic Acid Solutions and Frictional Behavior of Articular Cartilage. *Materials* **2020**, *13*, 2659. [CrossRef]
39. Wang, K.; Sun, X.H.; Zhang, Y.; Zhang, T.; Zheng, Y.; Wei, Y.C.; Zhao, P.; Chen, D.Y.; Wu, H.A.; Wang, W.H.; et al. Characterization of Cytoplasmic Viscosity of Hundreds of Single Tumour Cells Based on Micropipette Aspiration. *R. Soc. Open Sci.* **2019**, *6*, 181707. [CrossRef]
40. Hilšer, P.; Suchánková, A.; Mendová, K.; Filipič, K.E.; Daniel, M.; Vrbka, M. A New Insight into More Effective Viscosupplementation Based on the Synergy of Hyaluronic Acid and Phospholipids for Cartilage Friction Reduction. *Biotribology* **2021**, *25*, 100166. [CrossRef]
41. Ungai-Salánki, R.; Csippa, B.; Gerecsei, T.; Péter, B.; Horvath, R.; Szabó, B. Nanonewton Scale Adhesion Force Measurements on Biotinylated Microbeads with a Robotic Micropipette. *J. Colloid Interface Sci.* **2021**, *602*, 291–299. [CrossRef]
42. Wang, M.; Liu, Z.; Zhan, W. Janus Liposomes: Gel-Assisted Formation and Bioaffinity-Directed Clustering. *Langmuir* **2018**, *34*, 7509–7518. [CrossRef] [PubMed]
43. Ruozi, B.; Tosi, G.; Leo, E.; Vandelli, M.A. Application of Atomic Force Microscopy to Characterize Liposomes as Drug and Gene Carriers. *Talanta* **2007**, *73*, 12–22. [CrossRef] [PubMed]
44. Vorselen, D.; Piontek, M.C.; Roos, W.H.; Wuite, G.J.L. Mechanical Characterization of Liposomes and Extracellular Vesicles, a Protocol. *Front. Mol. Biosci.* **2020**, *7*, 139. [CrossRef] [PubMed]
45. Bates, D.; Mächler, M.; Bolker, B.; Walker, S. Fitting Linear Mixed-Effects Models Using Lme4. *J. Stat. Softw.* **2015**, *67*, 1–48. [CrossRef]
46. Marcotti, S.; Reilly, G.C.; Lacroix, D. Effect of Cell Sample Size in Atomic Force Microscopy Nanoindentation. *J. Mech. Behav. Biomed. Mater.* **2019**, *94*, 259–266. [CrossRef] [PubMed]
47. Cross, S.E.; Jin, Y.S.; Rao, J.; Gimzewski, J.K. Applicability of AFM in Cancer Detection. *Nat. Nanotechnol.* **2009**, *4*, 72–73. [CrossRef]
48. Fischer-Cripps, A.C. *Introduction to Contact Mechanics*, 2nd ed.; Mechanical Engineering Series; Springer: New York, NY, USA, 2011.
49. Ciulli, E.; Betti, A.; Forte, P. The Applicability of the Hertzian Formulas to Point Contacts of Spheres and Spherical Caps. *Lubricants* **2022**, *10*, 233. [CrossRef]
50. Johnson, K.L. One Hundred Years of Hertz Contact. *Proc. Inst. Mech. Eng.* **1982**, *196*, 363–378. [CrossRef]
51. Johnson, K.L. *Contact Mechanics*; Cambridge University Press: Cambridge, UK, 2004.
52. Popov, V.L. *Contact Mechanics and Friction*; Springer: Berlin/Heidelberg, Germany, 2017. [CrossRef]
53. Hertz, H. Ueber die Berührung fester elastischer Körper. *J. für Die Reine Und Angew. Math.* **1882**, *92*, 156–171.
54. Podio-Guidugli, P.; Favata, A. The Boussinesq Problem. In *Elasticity for Geotechnicians: A Modern Exposition of Kelvin, Boussinesq, Flamant, Cerruti, Melan, and Mindlin Problems*; Podio-Guidugli, P., Favata, A., Eds.; Springer International Publishing: Cham, Switzerland, 2014; pp. 79–114. [CrossRef]
55. Selvadurai, A.P.S. On Boussinesq's Problem for a Cracked Halfspace. *J. Eng. Math.* **2017**, *107*, 269–282. [CrossRef]
56. Selvadurai, A.P.S. On Boussinesq's Problem. *Int. J. Eng. Sci.* **2001**, *39*, 317–322. [CrossRef]
57. Landau, L.D.; Lifšic, E.M. *Theory of Elastic*, 3rd ed.; Course of Theoretical Physics; Elsevier Butterworth Heinemann: Amsterdam, The Netherlands, 2009.